Available online at www.sciencedirect.com
SCIENCE DIRECT®
Biochimica et Biophysica Acta 1697 (2004) 289–300
BIOCHIMICA ET BIOPHYSICA ACTA
BBA
www.bba-direct.com

Review

Structure, dynamics and interaction with kinase targets: computer simulations of calmodulin

Cheng Yang[a,1], Gouri S. Jas[a,b], Krzysztof Kuczera[a,*]

[a] *Department of Chemistry and Department of Molecular Biosciences, University of Kansas, 2010 Malott Hall, Lawrence, KS 66045 USA*
[b] *Higuchi Biosciences Center, University of Kansas, Lawrence, KS 66049 USA*

Received 29 September 2003; accepted 12 November 2003

Abstract

Calmodulin (CaM) is a small protein involved in calcium signaling; among the targets of CaM are a number of kinases, including myosin light chain kinases (MLCK), various CaM-dependent kinases and phosphorylase kinase. We present results of molecular dynamics (MD) simulations of 4-ns length for calmodulin in its three functional forms: calcium-free, calcium-loaded, and in complex with both calcium and a target peptide, a fragment of the smooth muscle MLCK. The simulations included explicit water under realistic conditions of constant temperature and pressure, the presence of counterions and Ewald summation of electrostatic forces. Our simulation results present a more complete description of calmodulin structure, dynamics and interactions in solution than previously available. The results agree with a wide range of experimental data, including X-ray, nuclear magnetic resonance (NMR), fluorescence, cross-linking, mutagenesis and thermodynamics. Additionally, we are able to draw interesting conclusions about microscopic properties related to the protein's biological activity. First, in accord with fluorescence data, we find that calcium-free and calcium-loaded calmodulin exhibit significant structural flexibility. Our simulations indicate that these motions may be described as rigid-body translations and rotations of the N- and C-terminal domains occurring on a nanosecond time scale. Our second conclusion deals with the standard model of calmodulin action, which is that calcium binding leads to solvent exposure of hydrophobic patches in the two globular domains, which thus become ready to interact with the target. Surprisingly, the simulation results are inconsistent with the activation model when the standard definitions of the hydrophobic patches are used, based on hydrophobic clefts found in the X-ray structure of calcium-loaded calmodulin. We find that both experimental and simulation results are consistent with the activation model after a redefinition of the hydrophobic patches as those residues which are actually involved in peptide binding in the experimental structure of the calmodulin–peptide complex. The third conclusion is that the calmodulin–peptide interactions in the complex are very strong and are dominated by hydrophobic effects. Using quasi-harmonic entropy calculations, we find that these strong interactions induce a significant conformational strain in the protein and peptide. This destabilizing entropic contribution leads to a moderate overall binding free energy in the complex. Our results provide interesting insights into calmodulin binding to its kinase targets. The flexibility of the protein may explain the fact that CaM is able to bind many different targets. The large loss of conformational entropy upon CaM:peptide binding cancels the entropy gain due to hydrophobic interactions. This explains why the observed entropic contribution to the binding free energy is small and positive, and not large and negative as expected for a complex with such extensive hydrophobic contacts.

Keywords: Calmodulin; Molecular dynamics simulation; Protein–peptide interaction; Kinase; Poisson–Boltzmann equation; Quasi-harmonic entropy calculation

1. Introduction

Calmodulin (CaM) is a ubiquitous calcium-binding protein of 148 residues found in all eukaryotic cells; CaM can bind and regulate various target enzymes in a Ca^{2+}-dependent manner [1,2]. Among the targets of calmodulin are a number of kinases, including myosin light chain kinase (MLCK), various CaM-dependent kinases and phosphorylase kinase as well as the plasma membrane calcium ATPase

Abbreviations: CaM, calmodulin; MLCK, myosin light chain kinase; smMLCK, smooth muscle MLCK; FRET, fluorescence resonance energy transfer; NMR, nuclear magnetic resonance; MD, molecular dynamics; ED, essential dynamics

* Corresponding author. Department of Chemistry, University of Kansas, 1251 Wescoe Hall Drive, Lawrence, KS 66045 USA. Tel.: +1-785-864-5060; fax: +1-785-864-5396.
E-mail address: kkuczera@ku.edu (K. Kuczera).
[1] Present address: Department of Biochemistry and Molecular Biophysics, University of Pennsylvania, Philadelphia, PA 19104 USA.

1570-9639/$ - see front matter © 2003 Elsevier B.V. All rights reserved.
doi:10.1016/j.bbapap.2003.11.032

[1,2].Three functional states of calmodulin have been characterized experimentally: calcium-free, calcium-loaded and with both calcium and a target peptide bound to the protein. Experimental structures of these forms have been determined by X-ray crystallography [3–7] and solution nuclear magnetic resonance (NMR) studies [8–10]. The protein consists of two Ca^{2+}-binding domains, each containing two helix-loop-helix EF hand motifs, separated by a mostly helical central linker region to form a dumbbell-like shape. Analysis of the experimental structures indicates that the binding of calcium to apo-CaM triggers a conformational change in which the two domains move further apart, the linker region connecting the domains becomes more helical and hydrophobic residues become exposed to solvent [1–3,7,10]. Besides the basic structural studies, a significant amount of experimental work has been devoted to the dynamics and interactions of CaM. Studies of the central linker in calcium-loaded CaM indicate that while it forms a single helix spanning residues 65–92 in the crystal [5], the region exhibits structural flexibility in solution [11–14]. The structural and dynamical differences between apo and calcium-loaded CaM have been investigated by a variety of methods, including small angle X-ray scattering (SAXS) [11], fluorescence resonance energy transfer (FRET) [14,15], fluorescence depolarization [14,15], and NMR relaxation [16]. In turn, investigations of the protein–peptide interactions have been carried out by methods including NMR [17,18], site-directed mutagenesis of the protein [19–22] and target peptide [23–25] as well as thermodynamic studies [26,27].

Previous computer simulations of calmodulin mostly focused on modeling the flexibility of the central helix [28–30]. The earliest studies without water [28] and with very limited solvation [29] revealed the possibility of central helix deformations. Bending of the isolated central helix and a limited bending of the linker in the whole protein were detected [30]. A 3-ns molecular dynamics (MD) study of calcium-loaded CaM with counterions in a 44-Å water sphere found unwinding of the central helix near Arg 74, a major reorientation of the two calcium-binding domains, and a rearrangement of α-helices in the N-terminus relative to the crystal structure [31]. Simulations of the solution dynamics of calcium-free and calcium-loaded forms of the N-terminal domain of CaM have also been performed [32]. CaM–peptide interactions present in the experimental structures were analyzed in a molecular modeling study [33]. This work indicated that the protein–peptide interface could be divided into two parts, with the core having a hydrophobic character, including four deep pockets able to accommodate bulky side chains, while the edges of the binding surface were negatively charged, interacting strongly with the basic peptide residues [33].

We have previously described 4-ns simulations of calcium-free CaM [34], calcium-loaded CaM [35] and the CaM:smMLCK peptide complex [36], performed under realistic conditions of constant temperature and pressure, in the presence of counterions and with Ewald treatment of electrostatic interactions. We present here a synthesis of simulation results for the three functional forms of CaM. The analysis of the previous simulations is expanded by a comparison of the essential dynamics (ED) parameters describing domain motions, a careful analysis of the solvent accessible surface areas (SASA) aimed at interpreting the CaM activation model, and quasi-harmonic entropy calculations of the strain induced by binding calcium and target peptide. The simulation results are tested by comparison with a wide range of experimental data and used to obtain valuable atomic-level insights into the properties of this important protein.

Our simulation results provide a fundamental understanding of the behavior of calmodulin in solution. Besides describing the structure and dynamics of the protein, we present an analysis of the thermodynamic driving forces involved in the formation of the CaM:smMLCK complex. This allows us to explain the unexpected observed value of the entropic contribution to the free energy of CaM:smMLCK binding in terms of a balance between favorable hydrophobic interactions and unfavorable conformational entropy loss. Overall, our findings are relevant to understanding of the mechanism of biological activity of calmodulin and its interactions with kinase targets.

2. Experimental procedures

The starting coordinates for the simulations were taken from the Protein Data Bank; the 1CLL crystal structure was used for calcium-loaded calmodulin [5], the minimized average NMR structure 1CFD for calcium-free CaM [9], and the X-ray structure 1CDL for the CaM:smMLCK peptide complex [7]. Missing residues and/or hydrogen atom positions were built in using the program CHARMM [37]. Each of the systems was neutralized by addition of sodium and chloride ions at close to physiological ionic strength and solvated in a bcc (truncated octahedral) cell based on a cube of side 92 Å with TIP3P model waters [38]. MD simulations at constant pressure of 1 atm and a constant temperature of 300 K were performed using the program CHARMM with version 22 all-atom topology and parameters [37,39]. The final simulation systems consisted of 35,347 atoms (including 11,007 water molecules) for the calcium-free, 35,387 atoms (including 11,953 water molecules) for the calcium-loaded, and 35,416 atoms (including 10,917 water molecules) for the CaM:smMLCK complex. The Particle-Mesh Ewald (PME) method was used to avoid truncation of electrostatic interactions [40]. SHAKE constraints were used to fix lengths of bonds involving hydrogen atoms [41], enabling integration of equations of motion with a 2-fs time step. Simulations were performed on SGI ORIGIN supercomputers at the University of Kansas and the National Center for Supercomputing Applications. Further simulation details may be found in Refs. [34–36].

ED analysis of the protein and peptide motions was performed by diagonalization of the covariance matrix describing the average fluctuations of the backbone atoms over trajectories from which effects of overall translations and rotations have been removed. The eigenvectors with the largest eigenvalues provided models for collective coordinates which best describe the calculated structural fluctuations [42,43]. To estimate the conformational entropies of the different forms of CaM, we have performed quasi-harmonic entropy calculations as described in Ref. [44]. This involved diagonalization of the mass-weighted covariance matrix describing average backbone atom fluctuations from trajectories of the systems with overall translations and rotations removed. To estimate the conformational entropy change upon CaM:smMLCK complex formation, analogous quasi-harmonic entropy calculations were performed for the separate smMLCK peptide, requiring generation of a trajectory for this system. This simulation was started at the helical structure extracted from the 1CDL PDB file [9], with one Na^+ and seven Cl^- counterions added to neutralize the system and provide a physiological ionic strength. The system was solvated in a 54-Å bcc cell with TIP3P waters. There were 7765 atoms altogether. Simulations were run for 2 ns on a DELL workstation under Linux. The remaining details were the same as for the protein simulations, see, e.g. Ref. [35]. In the simulation, the peptide reached an RMS deviation of 4 Å from the starting helical structure.

The interaction free energy within the CaM:smMLCK complex was calculated as described in Ref. [36]. The free energy involved electrostatic and nonpolar terms. The electrostatic term was calculated using the linearized Poisson–Boltzmann equation [45,46], as the difference between solvation free energies of the CaM:smMLCK complex and separated CaM and smMLCK peptide. Each solvation free energy was the difference between charging up a system in vacuum and in aqueous solution. A 0.5-Å grid was used, with dielectric constants of 1 for protein and vacuum, and 80 for water. The nonpolar term was a linear function of the change in solvent accessible surface area upon complex formation, with a microscopic surface tension of 19 cal/(mol $Å^2$) and an offset of 0.6 kcal/mol, corresponding to solute transfer between cyclohexane and water [46–48].

MD simulations and trajectory analysis were performed using the program CHARMM, versions 26 and 28 [37,39]. Running in parallel on 16 processors of an SGI ORIGIN supercomputer, generation of a 4-ns trajectory of solvated calmodulin took about 3 months of CPU time with the cutoff model, and about 5 months using the PME method. Color images and animations illustrating calmodulin structure and dynamics in solution may be viewed at our web site [49].

3. Results: structure and dynamics

The results of the MD simulations of the three forms of calmodulin are described below. For the sake of brevity, the system involving calcium-free calmodulin will be denoted by apo-CaM, the calcium-loaded protein by Ca-CaM and the complex of calcium-activated calmodulin with the smooth muscle MLCK peptide by CaM:smMLCK. A more complete description of the trajectories may be found elsewhere [34–36].

3.1. Overall structure and dynamics

The starting structures for the simulations of the three forms of calmodulin are shown in Fig. 1. When the complete systems were considered, the maximum backbone atom root-mean-square (RMS) deviations from the starting structures within the trajectories reached about 7 Å for apo-CaM, 5 Å for Ca-CaM and 2 Å for CaM:smMLCK. When overlaying only either the N-terminal or C-terminal domains, the RMS deviations from the starting structures were in the 1–2 Å range in all three simulations. Overlay of the peptide backbone coordinates only in CaM:smMLCK produced a 0.5-Å RMS deviation from the initial 1CDL structure.

The average backbone atom RMS atomic fluctuations were 3.2 Å for apo-CaM, 2.1 Å for Ca-CaM and 0.9 Å in CaM:smMLCK, after removal of overall translation and rotations. To remove the effect of domain motions in apo-CaM and Ca-CaM, we also calculated the RMS fluctuations within the domains around separate N- and C-terminal domain average structures; the results were about 1 Å in both cases. These last values are in good agreement with the 1-Å atomic fluctuations which may be calculated from the X-ray B-factors from the X-ray structures 1CLL and 1CDL, as well as the ca. 1 Å RMS position fluctuations within the sample of the 20 NMR models (1CFC) used to obtain the apo-CaM initial coordinates 1CFD.

Thus, the two domains of CaM remain stable, with internal structures close to experimentally determined ones. Since the overall RMS deviations tend to be significantly larger than the deviations of the substructures for apo-CaM and Ca-CaM, it is clear that rearrangements involving rigid-body motions of the domains occur in these two trajectories. In the case of CaM:smMLCK, both the peptide and protein remain close to the experimental structure and there appear to be no significant domain motions.

3.2. Hydrogen bonds

Hydrogen bonding patterns are an important feature of protein structure [50,51]. The secondary structure of the calmodulin domains found in the experimental starting structures was generally maintained in the simulations. Only in the apo-CaM simulation breaking of a hydrogen bond at the end of helix A and formation of additional hydrogen bonds at the ends of helices B and H were observed [34].

In the apo-CaM simulation an interdomain hydrogen bond was formed between side chains of Glu 11 and Lys

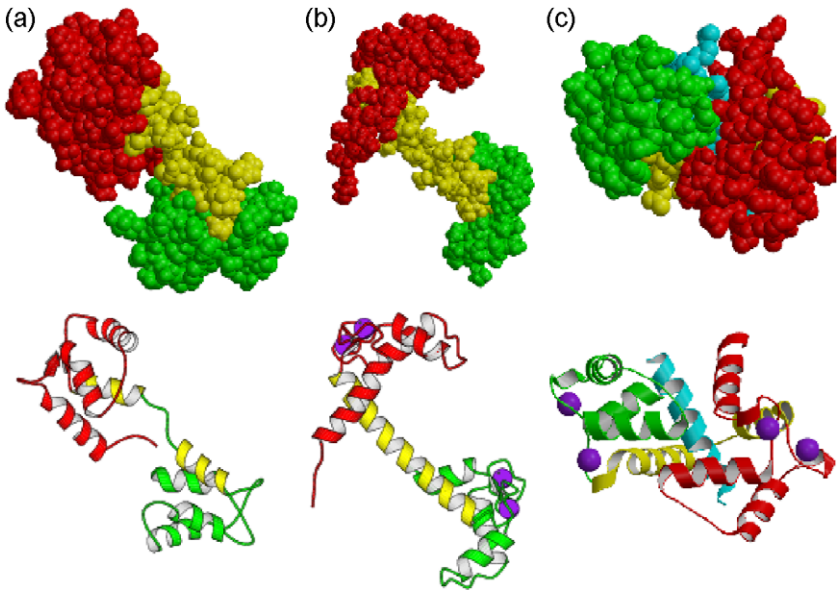

Fig. 1. Schematic representation of the three structural forms of calmodulin. (a) apo-CaM structure 1CFD [9]. (b) Ca-CaM structure 1CLL [5]. (c) CaM:smMLCK peptide complex structure 1CDL [7]. Each structure was shown as a cartoon and space-filling model. Colors: N-terminal domain—red; C-terminal domain—green; central linker—yellow; calcium ions—purple; smMLCK peptide—cyan.

115 after 2.5 ns. In the calcium-loaded trajectory, hydrogen bonds were formed between side chains of residues Glu 54...Arg 74 and Glu 82...Arg 86, while backbone hydrogen bonds Asp 80...Glu 84 and Ser 81...Ile 85 in the central linker were broken, reflecting the reorganization of the central linker region. In the CaM:smMLCK simulation, there were nine protein–peptide hydrogen bonds, in accord with the starting structure [7].

3.3. Interdomain linker

The interdomain linker region extends between residues 65 and 92 of CaM. In calcium-free calmodulin this region consists of helix D (residues 65–75), helix E (residues 81–92) and a connecting loop (residues 76–80) [9]. The structural statistics of the linker region are presented in Table 1. The secondary structure of the central linker remains unchanged during the apo-CaM trajectory, in agreement with the starting structure 1CFD. The angle between helices D and E fluctuates between 10° and 100°, with an average of 51°. The distance between the α carbons of residues 65 and 92 can be used as a measure of the length of the interdomain linker region. This distance fluctuates in the 34–45 Å range during the 4-ns apo-CaM simulation, demonstrating significant conformational flexibility. The trajectory average distance, 40 Å, is identical to the value found in the NMR starting structure 1CFD [9].

In the crystal structure 1CLL of calcium-loaded CaM the central linker region adopts a predominantly α-helical conformation [5], while NMR studies indicate the presence of disorder for residues 77–81 in solution [12,13]. The region comprising residues 80 to 85 undergoes a noticeable structural distortion in the Ca-CaM trajectory. This may be seen both in deviations of (ϕ,ψ) from ideal helical values and in breaking of two hydrogen bonds, Asp 80 to Glu 84 and Ser 81 to Ile 85. The partial loss of helical structure in the central helix agrees qualitatively with NMR solution studies [12]. In the 4-ns Ca-CaM trajectory the angle between the two helical fragments of the central linker ranged between 0° and 50°, with an average value of 16°, similar to the 15° in the crystal structure [5] (the angle of 0° corresponds to a straight helix). The range of values sampled by the central linker length was 39–43 Å with an average of 41 Å, identical to the 1CLL crystal value [5] and

Table 1
Central linker and domain distances and orientations

	apo-CaM		Ca-CaM		CaM:smMLCK	
	MD	Exp	MD	Exp	MD	Exp
Linker length, Å	40 (34–45)	40	41 (39–43)	41	26 (24–28)	24
Linker bend angle, °	51 (10–100)	23	16 (0–50)	15	103 (81–125)	113
Domain distance, Å	33 (29–39)	36	38 (34–41)	40	24 (22–25)	22
Calcium dihedral, °	61 (−2–108)	82	−126 (−154 – −90)	−136	104 (93–115)	107

Trajectory averages compared with values in experimental starting structures. In parentheses—range explored. Details of coordinates are described in text. The experimental starting structures are 1CFD [9] for apo-CaM, 1CLL [5] for Ca-CaM and 1CDL [7] for CaM:smMLCK.

close to the 40.5 Å expected for an ideal α -helix with a rise of 1.5 Å per residue.

In the CaM:smMLCK complex crystal structure 1CDL the interdomain linker region helices extend between residues 65–70 (helix D) and 77–92 (helix E). The helices retain their secondary structure in the 4-ns CaM:smMLCK trajectory. The interhelix angle exhibits fluctuations in the 81–125° range, with an average of 103°. The central linker length has a trajectory average value of 26 Å, slightly larger than the experimental value of 24 Å [7]. The linker length fluctuates in the 24–28 Å range during the 4-ns CaM:smMLCK trajectory.

3.4. Domain motions

The separation of the N- and C-terminal domains of calmodulin may be described by the distance between the domains centers-of-mass, while the relative orientation may be described by the virtual dihedral angle formed by the four calcium ions, or in the case of apo-CaM, the four calcium binding sites. These data are presented in Figs. 2 and 3 and in Table 1.

During the 4-ns apo-CaM trajectory, the interdomain distance fluctuated in the 29–39 Å range, with an average of 33 Å, somewhat smaller than the 36 Å found in the NMR-derived initial structure 1CFD [9] (Fig. 2, Table 1). The dihedral angle formed by the four calcium binding sites varied between −2° and 108°, with an average value of 61° (Fig. 3, Table 1). The value of this coordinate in the starting 1CFD structure is 82°, while the distribution of calcium dihedrals in the 20 model structures (PDB file 1CFC) used to generate 1CFD was between 16° and 164°. Thus, there is a significant, though not complete, overlap between simulated and NMR dihedral distributions.

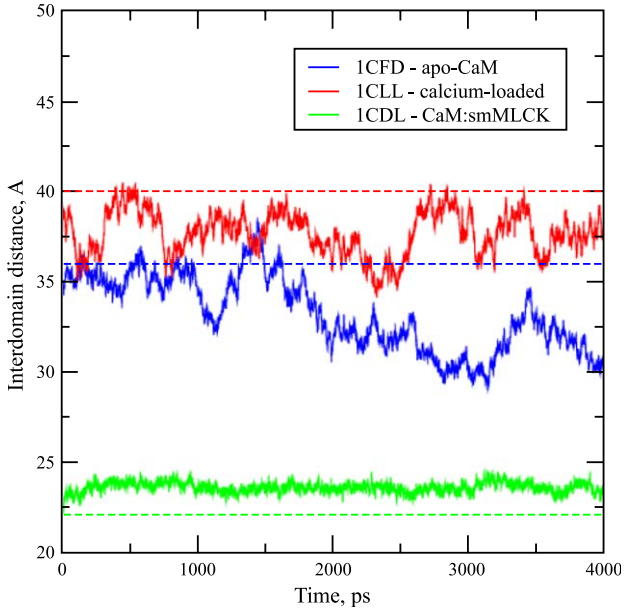

Fig. 2. Distance between the centers of mass of the N-terminal and C-terminal domains. Blue—apo-CaM trajectory; red—Ca-CaM trajectory; green—CaM:smMLCK trajectory. Dashed lines show values from starting experimental structures.

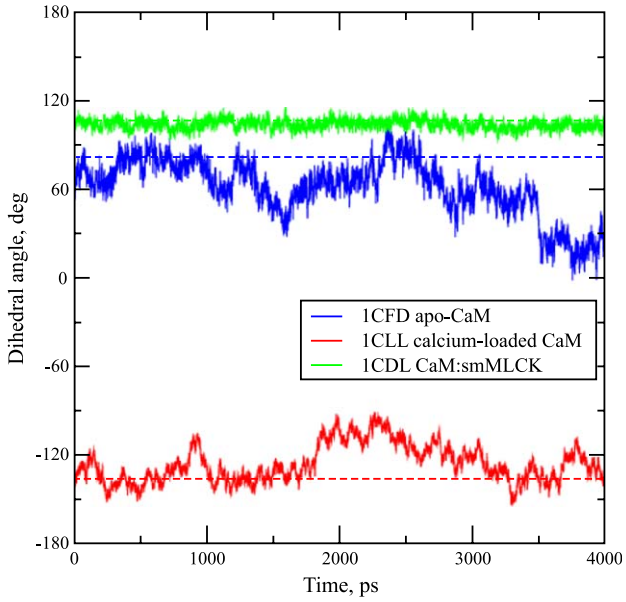

Fig. 3. The dihedral angle formed between the four calcium ions (Ca-CaM and CaM:smMLCK) and calcium binding sites (apo-CaM). Blue—apo-CaM trajectory; red—Ca-CaM trajectory; green—CaM:smMLCK trajectory. Dashed lines show values from starting experimental structures.

In the Ca-CaM trajectory the interdomain distance remained between 34 and 41 Å. The average distance was 38 Å, slightly smaller than the crystallographic value of 40 Å (Fig. 2, Table 1). The dihedral angle between the four calcium ions fluctuated around the crystallographic value of −136° throughout the simulation, exploring the range between −154° and −90° (Fig. 3, Table 1).

During the CaM:smMLCK simulation the interdomain distance falls in the 22–25 Å range, with an average value of 24 Å, somewhat larger than the 22 Å found in the initial X-ray structure 1CDL [7]. The dihedral angle formed by the four calcium ions stays between 93° and 115°, with an average value of 104°, quite similar to the 107° seen in the starting 1CDL crystal structure [7].

Thus, the simulation results indicate that large-scale domain motions occur in calcium-free and calcium-loaded CaM, while such motions are absent in the calmodulin–peptide complex.

3.5. Essential dynamics

We have performed an ED analysis to further characterize the large-scale collective motions of the protein [42,43]. In the apo-CaM trajectory the first mode contributed 69% of the total backbone mean-square fluctuations, while the first three modes contributed a total 88%. These modes describe rigid-body domain motions: bending of the central helix around a hinge located in its center, twisting around the interdomain axis and bending around an axis perpendicular

to that of the first mode, respectively. In the Ca-CaM trajectory the first three modes had identical character as described above, contributing 71% of the total protein backbone mean-square position fluctuations. For the CaM:smMLCK trajectory we found only one mode which had a significant contribution, 32%, to the overall atomic fluctuations. This mode appears to represent a breathing-type motion. The atomic fluctuations in CaM:smMLCK corresponded more to elastic deformations of a globular protein rather than to extensive relative motions of domains. Animations of the ED modes may be viewed at our web site [49].

A comparison of the ED of the three forms of CaM (Fig. 4) clearly shows the significantly larger fluctuation amplitudes in apo-CaM and Ca-CaM compared to the CaM:smMLCK complex. The ED modes with large amplitudes have significant projections on the direction of structural transitions between the three forms of CaM. For apo-CaM the first six ED modes have projections with absolute values of 0.10–0.38 on the apo-CaM to Ca-CaM structural transition. Analogously, the first six modes of Ca-CaM have projections with absolute values of 0.20–0.49 on the Ca-CaM to CaM:smMLCK transition. Finally, the locations of the average positions of the three forms of calmodulin indicate that apo-CaM, Ca-CaM and CaM:smMLCK do not form a linear progression but should rather be considered as equivalent structures in a triangular cycle.

Another measure of the flexibility of the three forms of calmodulin may be obtained by calculating the quasi-harmonic conformational entropy (Table 2). The calculated

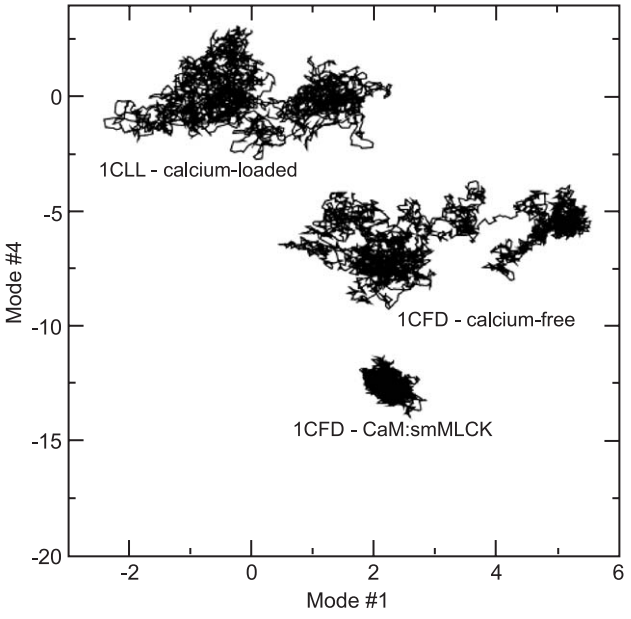

Fig. 4. Essential dynamics of the three forms of CaM. Fluctuations relative to trajectory average structures projected on ED modes 1 and 4 from the Ca-CaM trajectory. The three trajectories were oriented to a common frame, the 1CLL calcium-loaded structure.

Table 2
Quasi-harmonic conformational entropies calculated from backbone atom covariance in 4-ns trajectories of apo-CaM, Ca-CaM and CaM:smMLCK complex, and 2-ns trajectory of separate peptide

apo-CaM	Ca-CaM	CaM:smMLCK − p	CaM:smMLCK + p	smMLCK
671	617	585	661	103

For CaM:smMLCK complex separate calculations of protein with peptide (+p) and protein without peptide (−p) were performed. Values given are for *TS* term, with *S* the entropy and temperature $T = 300$ K. Units: kcal/mol.

values are 2.24, 2.05 and 1.95 kcal/mol K for the protein in the calcium-free, calcium-loaded and peptide-complexed states. These results correlate very well with the other measures of mobility, confirming that apo-CaM is the most and the peptide-bound form the least flexible.

3.6. Solvent accessible surface areas

SASA of the protein residues are computed with a probe radius of 1.6 Å. We have focused our attention on three aspects of the SASA of calmodulin in aqueous solution: total SASA of the protein, SASA of the methionine side chains, as well as the more general question of the hydrophobic patches.

The trajectory average SASAs for the protein as a whole tended to be systematically larger than the values from the corresponding experimental structures [34–36] (Table 3). This suggests that the simulated solution structures are somewhat looser than the starting structures. In the case of crystal structures 1CLL and 1CDL, this might be rationalized by the presence of crystal contacts [34]. In the case of the NMR solution structure 1CFD, the reason might be a subtle structural deformation introduced by the NMR structure determination protocol—while the direct NMR data correspond to a solution structure, the modeling of the data is still routinely performed for a system in vacuum [52].

The presence of nine methionine residues is an unusual feature of calmodulin. The methionines are all involved in peptide binding [7] and also are sites of protein oxidation [53,54]. The trajectory average SASA of methionine side chains are presented in Table 4. In the apo-CaM simulation these SASA are mostly in the 0–21Å^2 range, except for Met 76, for which the surface area is 51 Å^2. In the Ca-CaM trajectory most of the side chain SASA fall in the 21–26 Å^2 range, except for Met 71 and 72, which have SASA of 8 and 13 Å^2, respectively. The simulations reproduce the experi-

Table 3
Total SASA for three forms of calmodulin

apo-CaM		Ca-CaM		CaM:smMLCK + p		CaM:smMLCK − p	
MD	Exp	MD	Exp	MD	Exp	MD	Exp
10,253	9,801	10,506	10,277	10,304	9,407	8,931	8,083

Averages over the three 4-ns trajectories are compared with SASA of starting experimental structures. For the CaM:smMLCK complex calmodulin SASA in presence (+p) and absence (−p) of peptide is given. Experimental structures—as in Table 1. Units: Å^2.

Table 4
SASA of methionine side chains

	Apo-CaM		Ca-CaM		CaM:smMLCK −p		CaM:smMLCK +p	
	MD	Exp	MD	Exp	MD	Exp	MD	Exp
Met 36	8	0	31	28	30	20	0	3
Met 51	10	23	46	54	61	64	10	17
Met 71	0	5	8	37	58	42	8	0
Met 72	8	2	13	40	44	45	1	0
Met 76	51	32	38	70	108	83	92	48
Met 109	16	0	22	40	17	12	0	0
Met 124	7	1	38	59	63	40	0	0
Met 144	21	24	21	64	73	57	4	2
Met 145	1	0	43	58	57	66	0	0

Averages from 4-ns MD trajectories compared to values from the experimental starting structures (Table 1). Units: Å^2. For the Ala-Met-Ala peptide in an extended conformation the SASAs are 88, 44 and 171 Å^2 for the methyl group, sulfur atom and whole Met side chain, respectively, as calculated by CHARMM.

mental trend that SASA values of methionines are lower in apo-CaM than in calcium-activated CaM, seen in structures [9,5,35], oxidation rates [55] and NMR relaxation studies [56]. In the CaM:smMLCK trajectory, all nine methionines are involved in peptide binding, in accord with the starting 1CDL starting structure [7,36].

The concept of hydrophobic patches of calmodulin was originally based on the identification of hydrophobic clefts in the crystal structure of calcium-loaded calmodulin. It was proposed that two patches of 14 residues each get exposed to solvent upon calcium binding and that subsequently these patches are involved in interactions with the target peptides [1,3]. Surprisingly, our simulations predicted similar SASA of these "standard hydrophobic patches" in the apo-CaM and Ca-CaM trajectories [34]. Similar effects were obtained in independent simulations of the N-terminal domain of CaM using a different force field and simulation protocol [32]. This discrepancy in patch SASA behavior was rationalized by suggesting that crystal contacts in the vicinity of the patches could distort the surface accessibility in the calcium-loaded crystal structure [32,34]. Additionally, while analyzing the CaM:smMLCK simulation, we found that of the 14 residues in each standard patch, only five are actually involved in interactions with the peptide; these were four methionines and one phenylalanine in each patch (Phe 19 and Met 36, 51, 71 and 72 in the N-terminal, and Phe 92 and Met 109, 124, 144 and 145 in the C-terminal). This was true for both the 1CDL structure and our trajectory. In view of these discrepancies faced by the "standard hydrophobic patches", we decided to reexamine the solvent accessibility data using a different approach, starting from the experimental structure of the CaM:smMLCK peptide complex [7].

We calculated the CaM residue SASA in the 1CDL structure [7] in the presence of the peptide and with the peptide deleted. This led to the identification of 41 residues for which the increase in SASA upon peptide removal was more than 5 Å^2 (Fig. 5). On this list of residues which exhibit the largest contacts with the target peptide, 26 were hydrophobic, 11 were glutamates and 4 were polar (see Table 5 and Fig. 6). The set of hydrophobic residues was

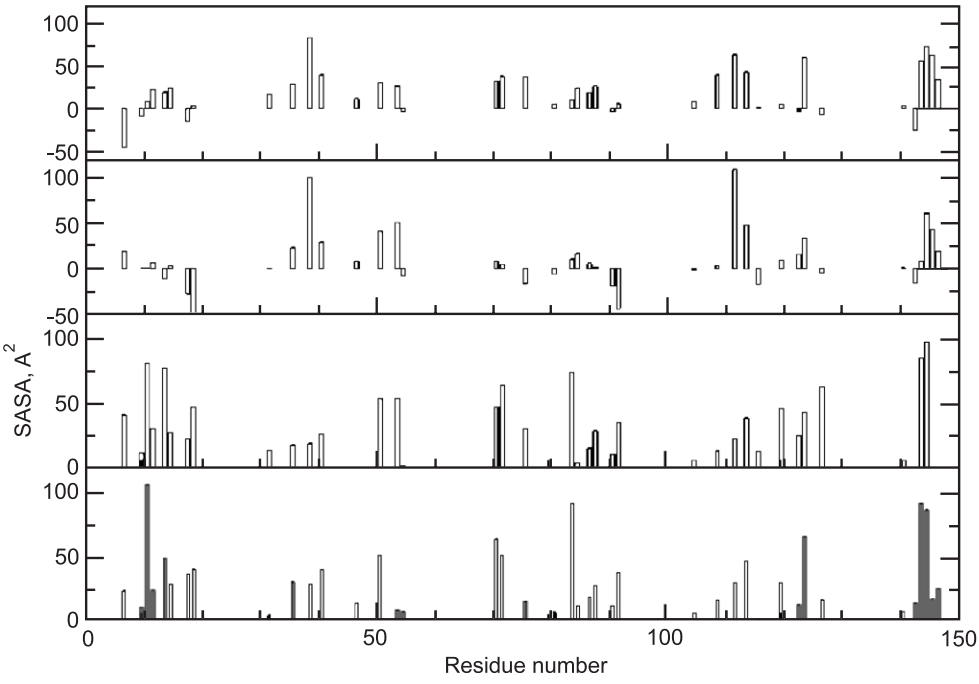

Fig. 5. CaM residue SASA changes upon calcium binding and surface areas of contact with peptide. (a) Experimental, SASA difference between 1CLL and 1CFD structures. (b) Simulations, difference between Ca-CaM and apo-CaM trajectory average SASA. (c) Experimental, surface area in contact with peptide in 1CDL structure. (d) Simulation, average surface area in contact with peptide in CaM:pep trajectory. Only values for the 41 CaM residues having largest contacts with the peptide in the CaM:smMLCK crystal structure 1CDL were shown for clarity.

Table 5
SASA for residues with largest contact with smMLCK peptide in the 1CDL structure [7]

	apo-CaM		Ca-CaM		CaM:smMLCK −p		CaM:smMLCK +p	
	MD	Exp	MD	Exp	MD	Exp	MD	Exp
Nonpolar	814	637	1061	1323	1226	1070	402	316
Charged/polar	1420	1385	1623	1556	1470	1342	968	797
Total	2234	2022	2684	2879	2696	2412	1370	1113

See text and Fig. 7. The nonpolar residues forming the redefined hydrophobic patches are: Ala 10, Phe 12, Ala 15, Leu 18, Phe 19, Leu 32, Met 36, Leu 39, Met 51, Val 55, Met 71, Met 72, Met 76, Ile 85, Ala 88, Val 91, Phe 92, Leu 105, Met 109, Leu 112, Leu 116, Met 124, Phe 141, Met 144, Met 145 and Ala 147. The charged and polar residues are: glutamates 11, 14, 47, 54, 84, 114, 120, 123 and 127, as well as Gln 41, Ser 81, Gln 143 and Thr 146. Units: Å^2.

quite different from the "standard hydrophobic patches", the only common elements being the five residues per patch described in the previous paragraph. For the 26 hydrophobic residues in our set, the trajectory average SASA were 814, 1061 and 1226 Å^2, respectively, for apo-CaM, Ca-CaM and CaM:smMLCK (without peptide), while the values from the corresponding experimental structures were 637, 1323 and 1070 Å^2, respectively (Table 5). Thus, using our new definition of hydrophobic patches, both experimental and simulation data are consistent with the generally accepted model of CaM action, in which calcium binding exposes to solvent a number of hydrophobic residues, priming the protein for target binding. The residue SASA changes upon calcium binding are shown in Fig. 5a and b, and may be compared with the residue contact areas with the peptide in Fig. 5c and d. Clearly, the patterns observed in the corresponding simulations and experimental data are highly similar. The correlation coefficients are 0.67 between the data in Fig. 5a and b, and 0.81 for Fig. 5c and d. The patterns of SASA change upon calcium binding and peptide contacts are not highly similar. While most of the hydrophobic residues in our new patches tended to increase their solvent accessibility upon calcium binding (see Table 5 for total SASA), in several cases decreases of SASA were found in both experimental and simulation results.

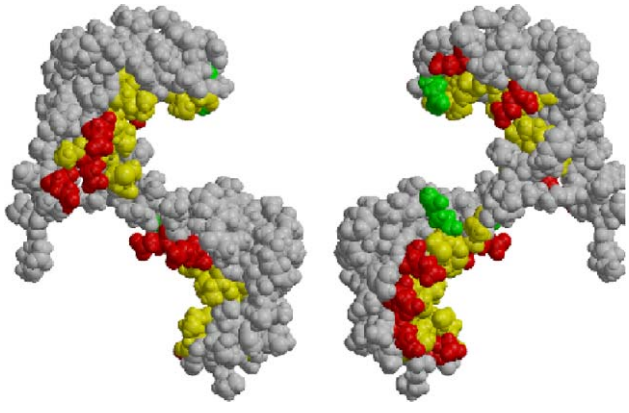

Fig. 6. View of the calcium-loaded CaM crystal structure 1CLL showing the 41 CaM residues having largest contacts with the peptide in the CaM:smMLCK complex 1CDL in color, the rest of residues in gray. Orange—residues which are part of the "standard hydrophobic patch"; yellow—other hydrophobic residues; red—glutamates; green—polar residues. (a) Front view, (b) back view.

4. Calmodulin–peptide interactions

We have performed calculations of the calmodulin–peptide interaction free energy using a continuum approach, which included an electrostatic term obtained using the Poisson–Boltzmann equation and a nonpolar or cavity term proportional to the SASA buried upon complex formation [36]. For a set of 100 structures sampled every 40 ps from our trajectory, the average electrostatic interaction free energy was −36 kcal/mol, with a standard deviation of 10 kcal/mol. The average cavity free energy was −64 kcal/mol with standard deviation of 2 kcal/mol. The average total interaction free energy was thus −100 kcal/mol. The simulated solution structure is strongly stabilized by both cavity and electrostatic terms. Analysis of the contributions of individual residues to the total electrostatic interaction free energy showed that the dominant effect was from seven negatively charged glutamates of CaM, Glu 7, 11, 14, 84, 114, 120 and 123, and from five positively charged basic residues of the peptide, Arg 3, Lys 4, Lys 7, Arg 13 and Arg 17. The trajectory average SASA buried upon complex formation was 1373 Å^2, of which a majority, 803 Å^2, is from nonpolar residues.

The experimentally determined free energy of the CaM:smMLCK peptide complex formation is about −11 kcal/mol, with an enthalpic (ΔH) and entropic ($-T\Delta S$) contributions of −16 and about +5 kcal/mol, respectively [26]. The large difference between the calculated free energy value of −100 kcal/mol and the experimental result may be explained through changes in structure and flexibility of both protein and peptide upon complex formation (Fig. 7). Calcium-loaded CaM by itself takes on an open, flexible structure with significant domain motions [12,13,15], while the peptide does not exhibit a definite secondary structure in solution [17]. In order to estimate the effect of flexibility change upon complex formation, we have calculated the quasi-harmonic conformational entropies of the CaM:smMLCK complex and the separate peptide and protein [44]. We used our CaM:smMLCK and Ca-CaM trajectories for the complex and free calcium-loaded protein, and a 2-ns simulation of the solvated peptide to evaluate the component entropies (Table 2). The calculated values of the TS term at a temperature $T = 300$ K were 661, 617 and 103 kcal/mol for the complex, separate protein and peptide, respectively, yielding an entropic contribution ($-T\Delta S$) to the binding

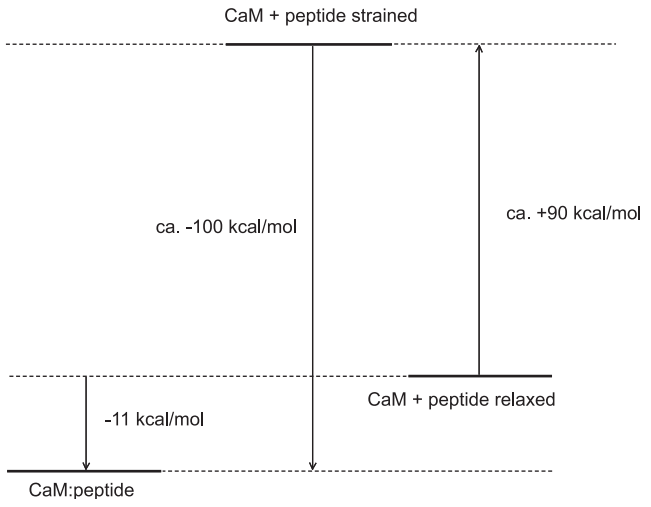

Fig. 7. The observed binding free energy of −11 kcal/mol for the CaM:smMLCK complex is represented as a sum of two large terms of opposite sign: a large unfavorable contribution of ca. +90 kcal/mol for forming the strained conformation of peptide and protein and a large favorable binding at fixed geometry of ca. −100 kcal/mol.

free energy of +59 kcal/mol. This value should be considered as a lower bound, since while the structural fluctuations of the CaM:smMLCK complex appear to be well sampled, it is probable that larger fluctuations, and thus larger values of conformational entropy, may be obtained by extending the Ca-CaM and separate smMLCK peptide trajectories. Additionally, the translational and rotational entropy loss upon complexation gives a $-T\Delta S$ contribution of +15 to +20 kcal/mol [57]. Thus, overall the conformational, translational and rotational entropy loss due to CaM:smMLCK peptide complex formation should contribute about +74 kcal/mol to the binding free energy. This effect explains a large part of the discrepancy between the calculated and measured binding free energy. The remaining part may be due to enthalpic effects, such as bringing together the negatively charged domains of CaM—the average domain–domain distance decreases by about 14 Å upon complex formation. The decomposition of the binding free energy into the preorganization of the protein and peptide into strained geometries followed by binding at fixed geometry is represented in Fig. 7.

The large calculated decrease in conformational entropy upon complex formation may be used to explain the unexpected value of the observed entropic contribution to the binding free energy. This quantity is small and positive, about +5 kcal/mol [26]. The large nonpolar surface area buried in the complex suggests that the hydrophobic effect should be an important factor in smMLCK peptide interactions with CaM. This effect is characterized by large negative entropic contributions $-T\Delta S$ to the free energy of binding [26]. The observed small entropic effect would thus be a result of cancellation between a decrease of the conformational entropy of the protein and peptide and an entropy increase due to hydrophobic interactions in the solvent.

Our simulation results show the presence of very strong protein–peptide interactions in the CaM:smMLCK complex. These interactions are mostly due to the burial of nonpolar surface area, with a secondary contribution from electrostatic interactions. This suggests that while electrostatic forces may be responsible for long-range attraction between CaM and the peptide, hydrophobic interactions are primarily responsible for the complex formation between CaM and a free unstructured peptide, in accord with experimental data [27]. These interactions induce significant conformational strain in the protein and peptide, leading to a moderate binding free energy and an unexpected value of binding entropy.

5. Comparison with experimental data

Our simulation results agree with a wide range of experimental data. The secondary structure within the domains agrees with NMR and X-ray structural information [5,7,9]. The disorder in the middle of the Ca-CaM central linker is in accord with solution NMR studies [12,13]. The presence of large-scale domain motions in apo-CaM and Ca-CaM agrees with results of cross-linking [58] and FRET [14,15]. The change to a more open and less flexible structure upon calcium binding is in accord with fluorescence [14,15] and X-ray scattering [11]. The changes in Met residue solvent accessibilities upon calcium binding are consistent with NMR relaxation [56] and oxidation rate experiments [55]. The important role in peptide binding of the glutamates and methionines of calmodulin and the basic amino acids and tryptophan of the peptide agree with structure and sequence analysis [7,59,60], and with mutagenesis studies of the protein [19–22] and peptide [23–25,33]. Analysis of the protein–peptide interactions is in accord with thermodynamic data [26,27].

There were some aspects of the simulations that were not in full agreement with experimental data. The trajectory backbone order parameters were systematically lower than observed values, indicating that the full range of motions of CaM has not yet been sampled [34–36]. The disorder in the middle of central linker of Ca-CaM extended over a smaller region than observed in NMR studies [13]. The data on methionine surface accessibility agreed qualitatively with the observed patterns, but showed some deviations in minor details [56,55]. The motion amplitudes seen in fluorescence experiments on calcium-loaded CaM were higher than those in our Ca-CaM trajectory [35]. Given the good agreement of simulations with the predominance of experimental data, we expect that these discrepancies should largely be eliminated when the time scale of the simulations is extended in the future. A more detailed comparison with experimental data is presented elsewhere [34–36].

The good overall agreement of our simulation results with experimental data suggests that we have captured much of the essential structural dynamics of the three forms of the

protein. It appears that our molecular model, the CHARMM force field with explicit solvent and Ewald summation of electrostatics, can provide a realistic representation of the structure and dynamics of calmodulin in solution.

6. Conclusions and perspectives

We have performed 4-ns MD simulations of three forms of calmodulin, calcium-free, calcium-loaded and in complex with the smMLCK peptide, in explicit solvent water including counterions and Ewald summation of electrostatic interactions. The simulation results allow us to describe the structure and dynamics of calmodulin in solution more fully than previously possible, test simulation results against a wide range of experimental data, and make interesting predictions about the microscopic properties related to CaM biological activity.

There are three main results of our calmodulin simulations that provide insight into the microscopic behavior of the protein in its three functional forms. The first is the presence of large-scale domain motions in calcium-free and calcium-loaded CaM. While the presence of these motions could be inferred from experimental data, our simulations make detailed predictions about their nature, namely that they involve rigid-body domain translations and rotations occurring on the nanosecond time scale. Thus, it appears that calmodulin is an example of a protein which does not populate a single, well-defined three-dimensional structure, but rather should be considered as sampling a range of structures. The second finding involves the nature of the hydrophobic patches of calmodulin. We found that the standard model of calmodulin activation, through exposure of hydrophobic patches to solvent upon calcium binding, can be supported by both experimental and simulation data only after a significant redefinition the hydrophobic patch regions. This conclusion could have been obtained by a more careful structural analysis involving just the experimental structures of the three forms of CaM. However, the need for such an analysis did not become evident until discrepancies between the activation model and simulation results were found. The standard patch definitions which do not include the information contained in the CaM:peptide complex structures are widely used. Our third major finding involves the nature of the CaM:smMLCK complex. We found very strong interactions in the complex, dominated by effects of burial of nonpolar surface area. These strong interactions induced significant conformational strain in the protein and peptide, leading to a moderate overall binding free energy. Our simulations suggest that hydrophobic interactions are the main force driving CaM:smMLCK complex formation. The unexpected observed value of the entropy of CaM:smMLCK binding may be explained by the cancellation of two large terms due to conformational strain and burial of nonpolar surface.

Other interesting conclusions from our simulations relate to the qualitative nature of the protein structure and dynamics. ED analysis indicates that the protein fluctuations have significant components along the structural transitions related to calcium and peptide binding. Also, the three forms of calmodulin are structurally equidistant, forming a triangular cycle rather than a linear progression. Another interesting aspect is that while maintaining a well-defined structure in the domains, the protein exhibits significant surface mobility, which may be seen in large fluctuations of the solvent accessibility of many residues.

Our simulations model a number of properties which are difficult to study by experimental methods alone. Taken together, the complementary computational and experimental data improve our understanding of the biological function of calmodulin and specifically of the interaction between calmodulin and its kinase targets. Thus, the flexibility of CaM and dominance of the relatively nonspecific hydrophobic interactions in the CaM:smMLCK peptide complex may be correlated with the ability of the protein to bind to a wide range of targets. Our results also support the predominant view that calcium binding exposes to solvent a number of hydrophobic residues of CaM, priming the protein for target binding. However, by combining experimental and simulation data, we propose a markedly different set of residues as constituents of the hydrophobic patches than previously considered. CaM dissociation from its targets at low calcium concentration may be explained by burial of the hydrophobic patches, which weakens the hydrophobic interactions that are the major stabilizing force of the CaM:smMLCK peptide complex. Finally, our simulations reveal the complex nature of CaM:smMLCK peptide interactions, with strong hydrophobic stabilization inducing large conformational strain.

In our future studies, we plan to extend the existing trajectories of the flexible states of calmodulin, in order to study the more long-term structural fluctuations. Further, we plan to address the question of the influence of methionine oxidation on the biological activity of the protein. This is a highly interesting question given that CaM contains nine methionines, and oxidation of some of these residues has been correlated with loss of protein activity due to aging and oxidative stress [54,55].

Acknowledgements

This research was supported by a grant from the American Heart Association (9951241Z). This work was partly supported by the National Computational Science Alliance under grant MCB990028N and utilized the ORIGIN 2000 array at the National Center for Supercomputing Applications at the University of Illinois at Urbana-Champaign. The authors also gratefully acknowledge the Center for Advanced Scientific Computing at the University of Kansas for time on the SGI ORIGIN 2400

computer system. We would like to thank Prof. Thomas Squier and Prof. Jeffrey Urbauer for helpful discussions. The figures containing molecular graphics were created using MolScript [61].

References

[1] A. Crivici, M. Ikura, Molecular and structural basis of target recognition by calmodulin, Annu. Rev. Biophys. Biomol. Struct. 24 (1995) 85–116.
[2] L.J.V. Eldik, D.M. Watterson, Calmodulin and Calcium Signal Transduction, Academic Press, San Diego, CA, 1998.
[3] Y.S. Babu, C.E. Bugg, W.J. Cook, Structure of calmodulin refined to 2.2 Å resolution, J. Mol. Biol. 204 (1988) 191–204.
[4] D.A. Taylor, J.S. Sack, J.F. Maune, K. Beckingham, F.A. Quiocho, Structure of a recombinant calmodulin from *Drosophila melanogaster* refined at 2.2-Å resolution, J. Biol. Chem. 266 (1991) 21375–21380.
[5] R. Chattopdhyaya, W.E. Meador, A.R. Means, F.A. Quiocho, Calmodulin structure refined at 1.7 Å resolution, J. Mol. Biol. 228 (1992) 1177–1192.
[6] S.T. Rao, S. Wu, K.A. Satyshur, K.-Y. Ling, C. Kung, M. Sundaralingam, Structure of paramecium tetraurelia calmodulin at 1.8 Å resolution, Protein Sci. 2 (1993) 436–447.
[7] W.E. Meador, A.R. Means, F.A. Quiocho, Target enzyme recognition by calmodulin: 2.4 Å structure of a calmodulin–peptide complex, Science 257 (1992) 1251–1255.
[8] M. Zhang, M. Tanaka, T.M. Ikura, Calcium-induced conformational transition revealed by the solution structure of apo calmodulin, Nat. Struct. Biol. 2 (1995) 758–767.
[9] H. Kuboniwa, N. Tjandra, S. Grzesiek, H. Ren, C.B. Klee, A. Bax, Solution structure of calcium-free calmodulin, Nat. Struct. Biol. 2 (1995) 768–776.
[10] M. Ikura, M. Clore, A.M. Gronenborn, G. Zhu, C.B. Klee, A. Bax, Solution structure of a calmodulin-target peptide complex by multidimensional NMR, Science 256 (1992) 632–638.
[11] D.B. Heidorn, J. Trewhella, Comparison of the crystal and solution structures of calmodulin and troponin C, Biochemistry 27 (1988) 909–915.
[12] M. Ikura, S. Spera, G. Barbato, L.E. Kay, M. Krinks, A. Bax, Secondary structure and side chain ^{1}H and ^{13}C resonance assignments of calmodulin in solution by heteronuclear multidimensional NMR spectroscopy, Biochemistry 30 (1991) 9216–9228.
[13] G. Barbato, M. Ikura, L.E. Kay, R.W. Pastor, A. Bax, Backbone dynamics of calmodulin studied by ^{15}N relaxation using inverse detected two-dimensional NMR spectroscopy: The central helix is flexible, Biochemistry 31 (1992) 5269–5278.
[14] Y. Yao, C. Schoeneich, T.C. Squier, Resolution of structural changes associated with calcium activation of calmodulin using frequency domain fluorescence spectroscopy, Biochemistry 33 (1994) 7797–7810.
[15] H. Sun, D. Yin, T.C. Squier, Calcium-dependent structural coupling between opposing globular domains of calmodulin involves the central helix, Biochemistry 38 (1999) 12266–12279.
[16] N. Tjandra, H. Kuboniwa, A. Bax, Rotational dynamics of calcium-free calmodulin studied by ^{15}N-NMR relaxation measurements, Eur. J. Biochem. 230 (1995) 1014–1024.
[17] M.R. Ehrhardt, J.L. Urbauer, A.J. Wand, The energetics and dynamics of molecular recognition by calmodulin, Biochemistry 34 (1995) 2731–2738.
[18] A.L. Lee, S.A. Kinnear, A.J. Wand, Redistribution and loss of side chain entropy upon formation of a calmodulin–peptide complex, Nat. Struct. Biol. 7 (2000) 72–77.
[19] A. Persechini, P.A. Stemmer, I. Ohashi, Localization of unique functional determinants in the calmodulin lobes of individual EF hands, J. Biol. Chem. 271 (1996) 32217–32225.
[20] T.A. Craig, D.M. Watterson, F.G. Prendergast, J. Haiech, D.M. Roberts, Site-specific mutagenesis of the á-helices of calmodulin, J. Biol. Chem. 262 (1987) 3278–3284.
[21] P.C. Weber, T.J. Lukas, T.A. Craig, E. Wilson, M.M. King, A.P. Kwiatkowski, D.M. Watterson, Computational and site-specific mutagenesis analyses of the asymmetric charge distribution on calmodulin, Proteins: Struct. Funct. Genet. 6 (1989) 70–85.
[22] M.O. Shoemaker, W. Lau, R.L. Shattuck, A.P. Kwiatkowski, P.E. Matrisian, L. Guerra-Santos, E. Wilson, T.J. Lukas, L.J. Van Eldrik, D.M. Watterson, Use of DNA sequence and mutant analyses and antisense oligonucleotides to examine the molecular basis of nonmuscle myosin light chain kinase autoinhibition, calmodulin recognition, and activity, J. Cell Biol. 111 (1990) 1107–1125.
[23] W.A. Findlay, M.W. Gradwell, P.M. Bayley, Role of the N-terminal region of the skeletal muscle myosin light chain kinase target sequence in its interaction with calmodulin, Protein Sci. 4 (1995) 2375–2382.
[24] T.J. Lukas, W.H. Burgess, F.G. Prendergast, W. Lau, D.M. Watterson, Calmodulin binding domains: characterization of a phosphorylation and calmodulin binding site from myosin light chain kinase, Biochemistry 25 (1986) 1458–1464.
[25] W.A. Findlay, S.R. Martin, K. Beckingham, P.M. Bayley, Recovery of native structure by calcium binding site mutants of calmodulin upon binding of sm-MLCK target peptide, Biochemistry 34 (1995) 2087–2094.
[26] P.L. Wintrode, P.L. Privalov, Energetics of target peptide recognition by calmodulin: a calorimetric study, J. Mol. Biol. 266 (1997) 1050–1062.
[27] R.D. Brockx, M.M. Lopez, H.J. Vogel, G.I. Makhatadze, Energetics of target peptide binding by calmodulin reveals different modes of binding, J. Biol. Chem. 276 (2001) 14083–14091.
[28] E.R. Mehler, J.R. Pascular-Ahuir, H. Weinstein, Structural dynamics of calmodulin and troponin C, Protein Eng. 4 (1991) 617–625.
[29] T. Vorherr, O. Kessler, A. Mark, E. Carafoli, Molecular dynamics simulations of calmodulin in the extended and in a bent conformation, Eur. J. Biochem. 204 (1992) 913–937.
[30] D. van der Spoel, B.L. de Groot, S. Hayward, H.J.C. Berendsen, H.J. Vogel, Bending of the calmodulin central helix: a theoretical study, Protein Sci. 5 (1996) 2044–2053.
[31] W. Wriggers, E. Mehler, F. Pitici, H. Weinstein, K.S. Schulten, Structure and dynamics of calmodulin in solution, Biophys. J. 74 (1998) 1622–1639.
[32] D. Vigil, S.C. Gallagher, J. Trewhella, A.E. Garcia, Functional dynamics of the hydrophobic cleft in the N-domain of calmodulin, Biophys. J. 80 (2001) 2082–2092.
[33] A. Afshar, L.S.D. Caves, L. Guimard, R.E. Hubbard, B. Calas, G. Grassy, J. Haiech, Investigating the high affinity and low sequence specificity of calmodulin binding to its targets, J. Mol. Biol. 244 (1994) 554–571.
[34] C. Yang, K. Kuczera, Molecular dynamics simulations of calcium-free calmodulin in solution, J. Biomol. Struct. Dyn. 19 (2002) 801–820.
[35] C. Yang, G.S. Jas, K. Kuczera, Structure and dynamics of calcium-activated calmodulin in solution, J. Biomol. Struct. Dyn. 19 (2001) 247–271.
[36] C. Yang, K. Kuczera, Molecular dynamics simulations of a calmodulin–peptide complex in solution, J. Biomol. Struct. Dyn. 20 (2002) 179–197.
[37] B.R. Brooks, R. Bruccoleri, B. Olafson, D. States, S. Swaminathan, M. Karplus, CHARMM: a program for macromolecular energy, minimization and dynamics calculations, J. Comput. Chem. 4 (1983) 187–217.
[38] W.L. Jorgensen, J. Chandrasekhar, J.D. Madura, R.W. Impey, M.L. Klein, Comparison of simple potential functions for simulating liquid water, J. Chem. Phys. 79 (1983) 926–935.
[39] A.D. MacKerell Jr., D. Bashford, M. Bellott , R.L. Dunbrack Jr., J.D. Field, M.J. Field, S. Fischer, J. Gao, H. Guo, S. Ha, D. Joseph-

McCarthy, L. Kuchnir, K. Kuczera, F.T.K. Lau, C. Mattos, S. Michnick, T. Ngo, D.T. Nguyen, B. Prodhom, W.E. Reiher III, B. Roux, M. Schlenkrich, J.C. Smith, R. Stote, J. Straub, M. Watanabe, J. Wiorkiewicz-Kuczera, M. Karplus, All-atom empirical potential for molecular modeling and dynamics studies of proteins, J. Phys. Chem. B 102 (1998) 3386–3616.

[40] C. Sagui, T.A. Darden, Molecular dynamics simulations of biomolecules: long-range electrostatic effects, Annu. Rev. Biophys. Biomol. Struct. 28 (1999) 155–179.

[41] J.P. Ryckaert, G. Ciccotti, H.J.C. Berendsen, Numerical integration of the cartesian equations of motion with constraints: molecular dynamics of *n*-alkanes, J. Comp. Physiol. 23 (1977) 327–341.

[42] A.E. Garcia, Nonlinear dynamics of proteins, Phys. Rev. Lett. 68 (1992) 2696–2699.

[43] A. Amadei, A.B.M. Linssen, D.M.F. Van Aalten, H.J.C. Berendsen, An efficient method for sampling the essential subspace of proteins, J. Biomol. Struct. Dyn. 13 (1996) 615–626.

[44] I. Andricioaei, M. Karplus, On the calculation of entropy from covariance matrices of the atomic fluctuations, J. Chem. Phys. 115 (2001) 6289–6292.

[45] K.A. Sharp, B. Honig, Electrostatic interactions in macromolecules: theory and application, Annu. Rev. Biophys. Biophys. Chem. 19 (1990) 301.

[46] B. Honig, A. Nicholls, Classical electrostatics in biology and chemistry, Science 268 (1995) 1144–1149.

[47] T. Simonson, A. Brunger, Solvation free energies estimated from macroscopic continuum theory: An accuracy assessment, J. Phys. Chem. 98 (1994) 4683–4694.

[48] T.J. Marrone, M.K. Gilson, J.A. McCammon, Comparison of continuum and explicit models of solvation: potential of mean force for alanine dipeptide, J. Phys. Chem. 100 (1996) 1439–1441.

[49] C. Yang, K. Kuczera, Images and animations of calmodulin dynamics in solution, http://oolung.chem.ukans.edu/~kuczera/1cll/1cll.html. 2001.

[50] D.J. Barlow, J.M. Thornton, Helix geometry in proteins, J. Mol. Biol. 201 (1988) 601–619.

[51] E.N. Baker, R.E. Hubbard, Hydrogen bonding in globular proteins, Prog. Biophys. Mol. Biol. 44 (1984) 97–179.

[52] B. Xia, V. Tsui, D.A. Case, H.J. Dyson, P.E. Wright, Comparison of protein solution structures refined by molecular dynamics simulations in vacuum, with a generalized born model and with explicit water, J. Biomol. NMR 22 (2002) 317–331.

[53] Y. Yao, D. Yin, G. Jas, K. Kuczera, T.D. Williams, C. Schöneich, T.C. Squier, Oxidative modification of a carboxyl-terminal vicinal methionine in calmodulin by peroxide inhibits calmodulin-dependent activation of the plasma-membrane Ca-ATPase, Biochemistry 35 (1996) 2767–2787.

[54] D. Yin, K. Kuczera, T.C. Squier, Sensitivity of carboxyl-terminus methionines in calmodulin isoforms to oxidation by HO modulates the ability to activate the plasma membrane ca-ATPase, Chem. Res. Toxicol. 13 (2000) 103–110.

[55] V.S. Sharov, C.S. Schoeneich, Diastereoselective protein methionine oxidation by reactive oxygen species and diastereoselective repair by methionine sulfoxide reductase, Free Radic. Biol. Med. 29 (2000) 986–994.

[56] T. Yuan, H. Ouyang, H.J. Vogel, Surface exposure of the methionine sidechains of calmodulin in solution. a nitroxide spin label and two-dimensional NMR study, J. Biol. Chem. 274 (1999) 8411–8420.

[57] A.V. Finkelstein, J. Janin, The price of lost freedom: entropy of biomolecular complex formation, Protein Eng. 3 (1989) 1–3.

[58] A. Persechini, R.H. Kretsinger, The central helix of calmodulin functions as a flexible tether, J. Biol. Chem. 263 (1988) 12175–12178.

[59] J. Goldberg, A.C. Nairn, J. Kuriyan, Structure of Ca^{++}/CaM-dependent protein kinase, Cell 84 (1996) 875–887.

[60] A.R. Rhoads, F. Friedberg, Sequence motifs for calmodulin recognition, FASEB J. 11 (1997) 331–340.

[61] P.J. Kraulis, MOLSCRIPT: a program to produce both detailed and schematic plots of protein structures, J. Appl. Crystallogr. 24 (1991) 946–950.